Research Article | Vol. 12, No. 2 / 1 February 2021 / Biomedical Optics Express 872
Biomedical Optics EXPRESS

Red and blue light in antitumor photodynamic therapy with chlorin-based photosensitizers: a comparative animal study assisted by optical imaging modalities

MIKHAIL KIRILLIN,[1,*] DARIA KURAKINA,[1] ALEKSANDR KHILOV,[1] ANNA ORLOVA,[1] MARIA SHAKHOVA,[1,2] NATALIA ORLINSKAYA,[1,2] AND EKATERINA SERGEEVA[1]

[1]*Institute of Applied Physics RAS, 46 Ulyanov St., Nizhny Novgorod, 603950, Russia*
[2]*Privolzhsky Research Medical University, 10/1 Minin and Pozharsky Sq., Nizhny Novgorod, 603950, Russia*
[*]*mkirillin@yandex.ru*

Abstract: The goal of this study is a comparative analysis of the efficiency of the PDT protocols for CT26 tumor model treatment in Balb/c mice employing red and blue light with both topical and intravenous administration of chlorin-based photosensitizers (PSs). The considered protocols include the doses of 250 J/cm^2 delivered at 660 nm, 200 J/cm^2 delivered at 405 nm, and 250 J/cm^2 delivered at both wavelengths with equal energy density contribution. Dual-wavelength fluorescence imaging was employed to estimate both photobleaching efficiency, typical photobleaching rates and the procedure impact depth, while optical coherence tomography with angiography modality (OCT-A) was employed to monitor the tumor vasculature response for up to 7 days after the procedure with subsequent histology inspection. Red light or dual-wavelength PDT regimes with intravenous PS injection were demonstrated to provide the most pronounced tumor response among all the considered cases. On the contrary, blue light regimes were demonstrated to be most efficient among topical application and irradiation only regimes. Tumor size dynamics for different groups is in good agreement with the tumor response predictions based on OCT-A taken in 24h after exposure and the results of histology analysis performed in 7 days after the exposure.

1. Introduction

Photodynamic therapy (PDT) is nowadays actively introduced into clinical practice as a technique for tumor treatment owing to both pronounced anticancer effect and good cosmetic results [1–10]. To enhance the potentialities of PDT, the development of novel protocols of PDT that efficiently employ spectral properties of photosensitizers (PSs) are of importance owing to wider capabilities of customizing the treatment tactics. For PSs with high absorption in different spectral ranges, the irradiation wavelength is a parameter of choice in a PDT procedure. Due to significant difference in the optical properties of biotissues in different bands of visible spectrum [11] the depth of the PDT procedure impact can be controlled by the choice of proper PS activation wavelength. Typical penetration depth of red light is much larger as compared to blue light [12–14] thus providing deeper action, while blue light is efficient for superficial impact.

Studies of PDT performance with employment of different wavelengths primarily report on ALA, MAL or protoporphyrins based PSs, since their absorption spectra feature a peak around 410 nm and bands in the green and red wavelength ranges. *In vitro* studies provide an opportunity to compare the efficiency of different PDT regimes at the cellular level [15,16]. Several studies report on multiple-wavelength PDT in *in vitro* versus *in vivo* tumor models [17–19]. In [17] the

#411518 https://doi.org/10.1364/BOE.411518
Journal © 2021 Received 1 Oct 2020; revised 8 Dec 2020; accepted 14 Dec 2020; published 15 Jan 2021

Biomedical Optics EXPRESS

efficiency of multiple-wavelength PDT with protoporphyrins was studied using several irradiation lines (405 nm, 505 nm, 545nm, 570 nm and 635 nm) in a single-wavelength mode and in all possible pairwise combinations. Antitumor action of ALA based-PDT in HT-29 human colon cancer cell line *in vitro* and in nude mice with implanted HT-29 cells [18] was shown to be the most efficient with the use of blue light (405 nm) and broadband white light as compared to red light (635 nm) irradiation. Greater antitumor effect of blue (405 nm) and green (525 nm) irradiation compared to red light (635 nm) of equal dose was also revealed during 5-ALA based PDT in animal model of peritoneal metastasis [19]. In normal tissues, differences in vascular damage were demonstrated after PDT with benzoporphyrin derivative for irradiation at 690 and 458 nm wavelengths [20]. The efficiency of different light sources in ALA- and MAL-based PDT was also evaluated in clinical studies, in particular in patients with basal cell carcinoma (BCC) in the setting of basal cell nevus syndrome (BCNS) [21–23]. In the paper [24] a comparative analysis of using red and green light in the ALA-based PDT of Bowen's disease is reported. Treatment was conducted with red (630 nm) and green (540 nm) light sources with equal fluence rate and was accompanied by monitoring of surface fluorescence excited by ultraviolet lamp with peak emission at 365 nm as well as contactless IR measurement of surface temperature.

Chlorin-based photosensitizers (PSs) are a wide class of PDT agents benefiting from two pronounced peaks in the absorption spectrum located in the red and the blue bands of the visible spectrum. However, a few wavelength comparison studies were reported with this type of PSs. Effects of low-dose PDT with blue light (405 nm), red light (660 nm) and their combination on normal tissue after topical application of chlorin-based PSs mimicking typical treatment procedures in antibacterial therapy and aesthetic medicine were reported in our previous paper [13]. A more pronounced response of normal tissues to blue light exposures as compared to red light exposures was demonstrated for both PDT and irradiation-only regimes. In the paper [25] the effect of chlorin e6 mediated photodynamic inactivation against biofilms related to periodontitis was evaluated depending on the light source wavelength (450 and 660 nm).

Another possible option in tuning the PDT protocol is the PS administration way. Most of the anticancer protocols use intravenous injection, however, topical administration is also considered as a method of choice for particular applications [26–28]. So far, no systemic comparison among topical administration PDT protocols as well as their comparison with intravenous injection protocols delivered in the same environment has been reported.

Optical imaging guidance of PDT has a high potential in clinic since it allows for non-invasive real-time monitoring of PDT and evaluating the post-treatment outcome of the procedure [29]. One of the imaging modalities implemented to assist PDT is the fluorescence imaging (FI) [29–31]. Owing to the fluorescence properties of PSs, FI modalities realize excellent theranostic combination with PDT [32–34]: they are employed for pre-treatment monitoring of PS distribution as well as for evaluation of PS photobleaching in course of PDT. PS photobleaching rate can serve as a dosimetric parameter of the procedure efficacy [32,33,35–39]. With the use of the PSs characterized by dual-wavelength excitation, FI benefits from simultaneous observation of both superficial and deeper layers [40–42]. The ratio of the fluorescence response values at the two excitation wavelengths provides the information about the PS penetration depth in case of topical PS administration [13]. However, this approach has not been used yet for evaluation of a PDT procedure performance. Optical imaging techniques additionally allow to trace tumor blood-flow alterations as a response to the PDT procedure. A number of optical modalities for monitoring tumor blood flow [43], including diffuse correlation spectroscopy and laser Doppler technique [44–48], were reported to monitor PDT procedures. Laser Doppler techniques allow monitoring of the flow changes with spatial resolution of hundreds μm with the probing depth limited by superficial tissue layer [43–46]. Diffuse correlation spectroscopy provides deeper probing, however, at the expense of spatial resolution [44, 47,48]. Optical coherence tomography (OCT), being implemented as an assisting imaging modality for PDT, can provide real-time

Biomedical Optics EXPRESS

monitoring of tumor structural changes [38]. OCT-based angiography (OCT-A) demonstrates promising results as a tool for the early evaluation of tumor response [49,50] providing spatial resolution below 20 μm, however, imaging depth is limited by ~ 1 mm. Tumor and peri-tumor vascular reaction assessed from OCT-A estimation of the perfused vessels average density allows to predict PDT clinical outcome (complete response/recurrence) as well as cosmetic outcome (normotrophic/hypertrophic scar) [51,52].

The aim of this study is a comprehensive comparative analysis of PDT protocols with chlorin-based PSs upon intravenous injection or topical administration employing both red and blue light for tumor treatment in *in vivo* animal experiment. In addition to traditional visual inspection and morphological studies the performed study employs non-invasive optical monitoring techniques, dual-wavelength FI and OCT-A, as well as local non-contact temperature measurements to evaluate the effect of treatment at all stages: prior to PDT, in the course of PDT procedure and in its follow-up of 7 days. A combination of the parameters collected from dual-wavelength FI data was used to analyze the effect of PDT in various treatment regimes, and OCT-A imaging performed in 7 days after treatment allowed to predict the tumor response verified visually and histologically.

2. Materials and methods

2.1. Animals

The study was performed on tumor model of murine colon carcinoma CT26 in 2-months-old female Balb/c mice ($n = 32$). Cells in the amount of 5×10^5 in 100 μl of PBS were injected subcutaneously into the outer side of the left shin. The tumor inoculation area was shaved prior to injection; in the following experiment the tumor site was additionally shaved if necessary to avoid artefacts during treatment and optical monitoring. The developed tumor model was subject to treatment in 7 days after inoculation when its linear size reached 3-5 mm. The skin thickness on the top of the tumor was evaluated around 200 μm based on structural OCT data and morphological information, which is in a good agreement with previously reported data [53]. Prior to topical PS application and the PDT procedure the animals were narcotized with the intramuscular injection of the mixture of 40 mg/kg Zoletil (Valdepharm, France) and 10 mg/kg XylaVet (Alpha-Vet Veterinary Ltd., Hungary). The animal studies were approved by the Ethics Committee of Privolzhsky Research Medical University (Protocol #7, 03.07.2017).

2.2. PDT protocols design

The study aimed at comparative analysis of antitumor PDT protocols with both intravenous injection and topical application of chlorin-based PSs employing irradiation with red and blue light alone or in combination. The exposures with the doses of 250 J/cm^2 delivered with red light ($\lambda = 660$ nm), 200 J/cm^2 delivered with blue light ($\lambda = 405$ nm), and 250 J/cm^2 delivered with combination of red and blue light in equal doses were considered. The nomenclature of the studied protocols is summarized in Table 1. The chosen doses are within the typical oncological range of 100-600 J/cm^2 [54]. Smaller dose for the blue light only regime and lower fluence rate for blue light illumination are aimed at avoiding excessive tumor heating. According to the spectra measured in [14], the 6-fold (blue to red) difference in absorption coefficient μ_a and 3-fold (blue to red) difference in reduced scattering coefficient μ_s' is observed for cutaneous murine tumor (with account of skin), thus resulting in about 4-fold difference (red to blue) in penetration depth estimated as $\delta = 1/\sqrt{3\mu_a(\mu_a + \mu_s')}$. Since the absorption of blue light primarily occurs in superficial layers, the absorbed dose accumulated in this volume for the blue light procedure exceeds that for the red light procedure, so the total dose was decreased to diminish this effect. In the dual-wavelength regime the red light dose is delivered first followed by the blue light dose, in

Biomedical Optics EXPRESS

order to avoid the effect of alterations in superficial tissues properties that may be induced by excessive absorption of blue light.

Table 1. Nomenclature of the employed PDT protocols and animal groups

Protocol abbreviation	Photosensitizer	Delivered dose	Fluence rate	Number of animals
PDT r250-i	"Fotolon" (Russia), intravenous injection	250 J/cm^2 @660 nm	200 mW/cm^2	3
PDT b200-i		200 J/cm^2 @405 nm	100 mW/cm^2	3
PDT rb250-i		125 J/cm^2@660 nm + 125 J/cm^2@405 nm	200 mW/cm^2 @660 nm + 100 mW/cm^2 @405 nm	3
PDT r250-t	"Revixan" (Russia), topical application	250 J/cm^2 @660 nm	200 mW/cm^2	3
PDT b200-t		200 J/cm^2 @405 nm	100 mW/cm^2	3
PDT rb250-t		125 J/cm^2@660 nm + 125 J/cm^2@405 nm	200 mW/cm^2 @660 nm + 100 mW/cm^2 @405 nm	3
IRR r250	No photosensitizer	250 J/cm^2 @660 nm	200 mW/cm^2	3
IRR b200		200 J/cm^2 @405 nm	100 mW/cm^2	3
IRR rb250		125 J/cm^2@660 nm + 125 J/cm^2@405 nm	200 mW/cm^2 @660 nm + 100 mW/cm^2 @405 nm	3
Control (untreated)	No photosensitizer	No exposure	No exposure	5

In the protocols with intravenous injection, Fotolon PS (Vetagrand, Russia) was administered intravenously in the amount of 5 mg/kg two hours prior to PDT procedure [54–56]. In the protocols with topical application, a PS gel Revixan (Revixan Ltd., Russia) containing 0.1% of pure chlorin e6 [12] was applied topically in the amount of ~0.1 ml and was distributed evenly with a cotton swab to cover all the tumor surface (approx. 2 cm^2); in 30 minutes after application the rest of the PS was removed from the tumor surface, also with a cotton swab. Prior to the PDT procedure all the surrounding tissues except the treated area were covered by a reflecting tape to avoid their direct irradiation. During the application period and after the PDT procedure mice were kept in darkened cages. The irradiation was performed with the PDT device "Harmonia" (Laser MedCenter Ltd., Russia) equipped with LED arrays with the wavelengths of 405 and 660 nm, the fluence rate at the tissue surface was 200 and 100 mW/cm^2 for wavelengths of 660 and 405 nm, respectively. The irradiation spot size was 9 mm in diameter.

Reference groups included control group (no exposure, natural tumor growth), and irradiation-only groups, in which the tumors were subject to the same light exposure but without PS administration. Each PDT and irradiation-only group consisted of 3 animals, control group included 5 animals.

Dynamics of the tumor growth was chosen as one of the criteria of PDT efficiency. In this connection, each tumor was measured in three dimensions prior to the procedure, and then each day after the procedure during 7 days in total. It was assumed that 7 days is a sufficient period for detection of the difference in the dynamics of tumor development. Assuming tumor shape to be close to an ellipsoid, tumor volume was calculated as

$$V = \frac{4}{3}\pi\frac{a}{2}\frac{b}{2}\frac{c}{2}, \tag{1}$$

Biomedical Optics EXPRESS

where a, b, and c are the measured length, width and height of the tumor, respectively. In order to quantify the effect of the considered treatment protocols on the tumor growth, we introduced the tumor growth inhibition factor (TGI) calculated as:

$$TGI = \frac{\bar{V}_c - \bar{V}}{\bar{V}_c} \cdot 100\% \tag{2}$$

where $\bar{V}_c$ is the average volume of tumor in the control group at a given time point, while $\bar{V}$ is the average tumor volume in the particular treatment group at the same time point. For the control group this index is equal to zero indicating no tumor growth suppression. Due to differences in the individual tumor growth dynamics, this index may vary in time for a particular group.

2.3. Tools for PDT monitoring

Dual-wavelength fluorescence imaging. Monitoring of PS accumulation in the tumor and its photobleaching in the course of PDT procedure was performed by the custom-made dual-wavelength fluorescence imaging device (IAP RAS, Russia) with probing wavelengths of 405 and 660 nm [41,57] corresponding to the absorption bands of chlorin e6, while fluorescence detection was performed in the range of 702-842 nm. The device provides two-dimensional fluorescence images of the target area at both excitation wavelengths registered with a 12-bit CCD camera. The power of the probing light sources is 1.9 and 1.1 mW at 405 and 660 nm, respectively, with exposure time for each frame below 0.5 s. Fluorescence imaging was performed prior to PDT and in the course of PDT procedure. The drop in the fluorescence signal indicating PS photobleaching was considered as the indicator of the procedure efficiency. For quantitative characterization, the photobleaching efficiency PE and fluorescence signal ratio R_λ were calculated as

$$PE = \frac{I_1 - I_2}{I_1} \cdot 100\%, \; R_\lambda = \frac{I_{660}}{I_{405}}, \tag{3}$$

where I_1 and I_2 are fluorescence intensities averaged over the region of interest (ROI) before and after PDT procedure, respectively, and I_{660} and I_{405} are current fluorescence intensities averaged over ROI detected at excitation wavelengths of 660 and 405 nm, respectively. In order to estimate the parameters of photobleaching kinetics in the given exposure regime, the fluorescence decay curve versus the delivered light dose D at each excitation wavelength was fitted by a bi-exponential function [58,59]:

$$I_k(D) = A^{(1)} e^{-d^{(1)}D} + A^{(2)} e^{-d^{(2)}D}, \tag{4}$$

where I_k is the intensity of fluorescence excited at a certain wavelength ($k = 405$, 660), $A^{(1),(2)}$ and $d^{(1),(2)}$ are the amplitudes and the photobleaching rate constants, respectively.

Optical coherence tomography. OCT-1300E device (IAP RAS, BioMedTech Ltd., Russia) operating at the central wavelength of 1300 nm and providing 3D OCT imaging with axial spatial resolution of 15 μm combined with OCT-angiography was employed to monitor structural and functional changes after the light exposure with or without PS. OCT-angiography concept implemented in the device is based on the analysis of decorrelation of OCT image speckle pattern induced by blood flow within the tissue vasculature [60,61]. The device is equipped with the contact probe which pressure to the tissue was controlled by a custom-designed holder to avoid effects of tissue compression on OCT images [62]. OCT imaging of the target area was performed prior to and immediately after the exposure, and in 1, 4 and 7 days after the procedure (in 24, 96 and 168 hours, respectively).

Temperature measurements. Since an excessive increase of the tumor temperature during the procedure may induce hyperthermia effect [63–65], monitoring of the surface temperature was performed in the treatment site prior to and immediately after the light exposure by non-contact IR-thermometer Optris (Germany) characterized by the accuracy of 0.1 K. Individual temperature changes were calculated to estimate the possible effect of hyperthermia during treatment.

Biomedical Optics EXPRESS

2.4. Histopathology studies

Biopsy samples were taken from the tumor sites in 7 days after PDT procedure following OCT examination and were further subjects for H&E staining. Morphological studies were performed by Leica DM 2500 microscope. Tumor response to the treatment was evaluated by a qualified morphologist in accordance with 4-grade scoring system accounting for the presence and the percentage of necrotic areas, hemorrhages, destroyed vessels, cells with pathologic mitosis, etc. Detailed description of the employed classification based on the histology inspection results is given in Table 2.

Table 2. Morphological criteria for different tumor response scores

Criterion	Grade 1	Grade 2	Grade 3	Grade 4
Necrosis area	5-10%	15-20%	20-25%	above 30%
Cells dystrophic alterations	+	++	+++	+++
Vessel destruction (microcirculation interruption)	+	+++	+++	+++
Inflammation	-	+	++	++
Number of tumor cells	high	average	average	low
Proliferation of connective tissue	-	+	++	+++
Hyalinosis	-	-	+	++
Increase of mitotic activity	-	+ (single within field of view x400)	++ (below 10 within field of view x400)	+++ (above 10 within field of view x400)
Presence of pathological mitoses and giant cells	-	-	+ (singular occurrences within field of view x400)	++ (above 5 within field of view x400)

Grade 1 corresponds to the primarily unaltered tumor tissues, however, single dystrophic and necrobiotic alterations may present due to natural excessive tumor development (spontaneous necrosis). In stromal tissue microcirculation disorders manifested by hemorrhages may present together with the focal proliferation of connective tissue and the enhancement of cell mitosis.

Grade 2 corresponds to the alteration in typical tumor morphologic structure manifested by dystrophic cell alterations, focal necrosis, and focal proliferation of connective tissue. Weak inflammatory reaction presents and is manifested by the round-cell infiltration together with the microcirculation interruption manifested by the destruction of capillaries. Increase of mitotic activity of tumor cells is observed as a reaction to the treatment accompanied by the presence of pathologic mitosis and formation of giant cells.

Grade 3 includes pronounced alterations in typical tumor structure as a result of massive necrosis, significant microcirculation interruption and connective tissue proliferation. Pronounced inflammatory reaction presents and is accompanied by the increased mitotic activity of tumor cells with pathologic mitosis and giant cells together with the microcirculation interruption manifested by the destruction of capillaries.

Grade 4 indicates destruction of tumor tissue and massive necrosis, complete elimination of tumor cells is possible. Proliferation of connective tissue is observed together with hyalinosis. Tumor vasculature is destroyed. Possibly preserved tumor tissue contains numerous pathologic mitoses and giant cells.

Biomedical Optics EXPRESS

3. Results and discussion

3.1. Fluorescence and temperature monitoring

Figures 1(a),(c) show the autofluorescence images of murine leg with inoculated tumor acquired at the two excitation wavelengths. The figure demonstrates that the level of autofluorescence is negligible compared to PS fluorescence. Figuresw 1(b),(d) depict fluorescence images of murine leg after topical application of PS and removal of its excess from the skin surface after 30-minutes exposition exhibiting high level of fluorescence signal (the mouse is covered with a reflecting tape with a hole in the tumor area). Monitoring of PS accumulation in the tumor upon intravenous injection observed by means of FI is shown in Fig. 2. Fluorescence imaging clearly demonstrates the contrast in accumulation of PS in the tumor with respect to the surrounding normal tissues. Dynamics of the fluorescence response from the tumor area (averaged over ROI indicated by dashed contour) during PS accumulation for excitation at the wavelengths of 405 and 660 nm is shown in Fig. 2(i) and the plateau in the accumulation is observed after 1 hour. As shown in [55], highest accumulation of Fotolon PS in murine tumor occurs in 2-4 hours after injection, which is in agreement with our observations and confirms that the chosen accumulation interval of 2 hours was the optimal one.

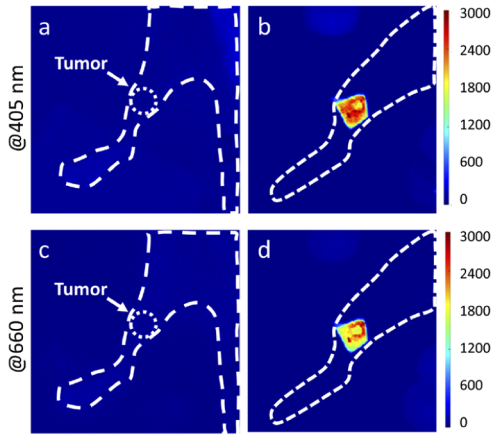

Fig. 1. Autofluorescence images of a Balb/c mouse leg with inoculated CT26 tumor (a,c) and fluorescence images of the murine leg covered with a reflecting tape in 30 minutes after PS topical application and removal of excessive PS (b,d) acquired at the excitation wavelengths of 405 (a,b) and 660 (c,d) nm. Dashed contour shows the position of the mouse leg.

PS photobleaching kinetics in the course of PDT procedure is one of the predictive factors of the efficiency of photodynamic reaction [66]. Figure 3 shows typical kinetics curves registered in tumor ROI in the course of PDT for different regimes with intravenous injection and topical administration for both excitation wavelengths together with the bi-exponential fitting curves in the form (4). For the case of intravenous injection, the accumulation of PS in tissues occurs due to microcirculation. In the ROI, PS is contained mainly in tumor and, to a lesser extent, in the skin covering the tumor; therefore, superficial layers contain less PS as compared to topical administration. In the case of blue light irradiation (PDT_b200-i) photobleaching occurs primarily in the skin and in the superficial tumor region. The volume under exposure corresponds to the probing volume of blue-light excited fluorescence ($\lambda = 405$ nm), while the probing volume of red-light excited fluorescence ($\lambda = 660$ nm) is larger, which is demonstrated by higher fluorescence level of the latter by the end of the PDT procedure. The PDT_r250-i procedure provides a deeper impact compared to blue exposure, which is detected by almost the

Biomedical Optics EXPRESS

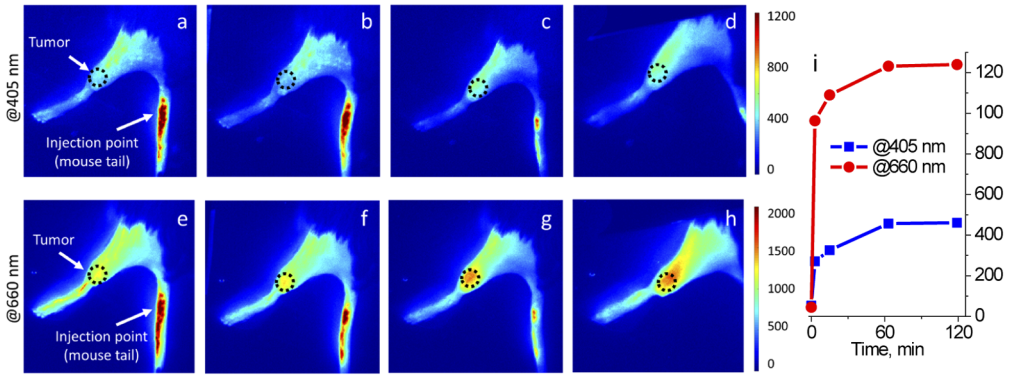

Fig. 2. Fluorescence images of a Balb/c mouse leg with inoculated CT26 tumor in 3(a,e), 15 (b,f), 60 (c,g) and 120 (d,h) minutes after intravenous PS injection acquired at the excitation wavelengths of 450 (a-d) and 660 (e-h) nm and corresponding PS accumulation dynamics within the tumor ROI after intravenous injection (i).

same fluorescence decay both for red and blue excitation wavelengths. For topical application protocols, the PS accumulation occurs primarily in superficial layers well sensed by both blue and red light excitation, so both excitation wavelengths demonstrate close dynamics. Since the absorption of PS at 405 nm is higher, PDT_b200-t procedure demonstrates more efficient photobleaching as compared to PDT_r250-t. Dual-wavelength regimes examples are not shown: they primarily repeat red light regimes as the red light fraction is delivered first and governs the fast part of the fluorescence kinetics.

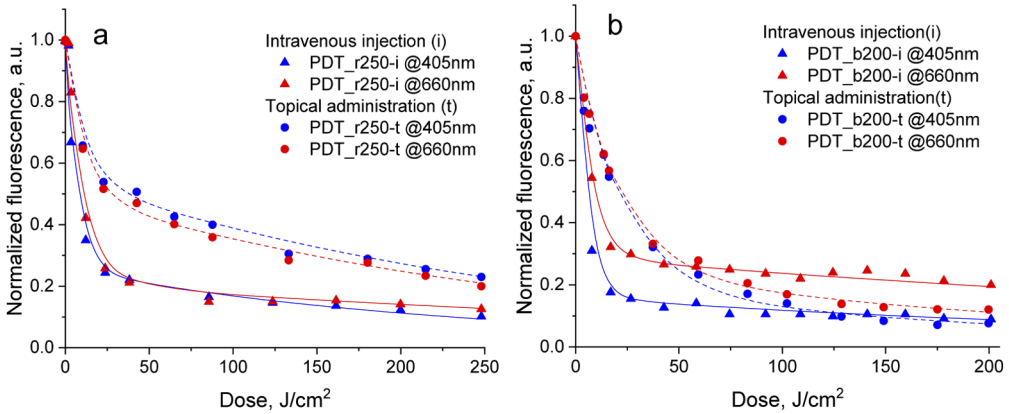

Fig. 3. Typical photobleaching kinetics registered by dual-wavelength (@405nm and @660 nm) fluorescence monitoring: normalized intensity of PS fluorescence in the course of PDT procedures with red (a) and blue (b) light regimes. Dots correspond to the measured fluorescence intensity. The bi-exponential fit (solid line for intravenous injection and dashed line for topical administration) calculated by Eq.(4) is given for each measured kinetics.

The photobleaching rate (PR) constants $d^{(1)}$ and $d^{(2)}$ calculated from fluorescence decay curves are summarized for all regimens and fluorescence excitation wavelengths in Fig. 4(a),(b). It is a general observation that $d^{(1)}$ exceeds $d^{(2)}$ by about an order of magnitude among all groups related to the same PS application mode (intravenous or topical), as the low-dose section of each kinetics curve is characterized by significantly faster decay than the rest of the curve. The values of the "fast" PR constant $d^{(1)}$ are close for red-light and dual-wavelengths exposures and

Biomedical Optics EXPRESS

amount about $d^{(1)} \cong 0.1$ cm^2/J, however, for blue-light exposure the fast kinetics is different: for PDT_b200-i regime $d^{(1)}$ is reliably higher, while for PDT_b200-t regime $d^{(1)}$ is reliably smaller than typical values for red-light containing PDT regimes. Note that when the photobleaching effect is observed by the fluorescence detection *in vivo*, estimation of "true" photobleaching rate is complicated by the influence of absorption and scattering on the irradiation density and, thus, non-equal photobleaching at different depths [66]. It is seen from Fig. 3 that the amplitude of "slow" kinetics characterized by the rate $d^{(2)}$ is larger for the regimens with topical PS administration, and $d^{(2)}$ values are generally higher in this case. This can be explained by the difference in the PS concentration and distribution in the exposed tissue volume for the two ways of PS administration, and therefore, its differing in-depth profile change in the course of photobleaching, and probably by the difference in oxygen concentration in superficial and deeper biotissue layers which may influence the photobleaching rate during photochemical reaction [67,68].

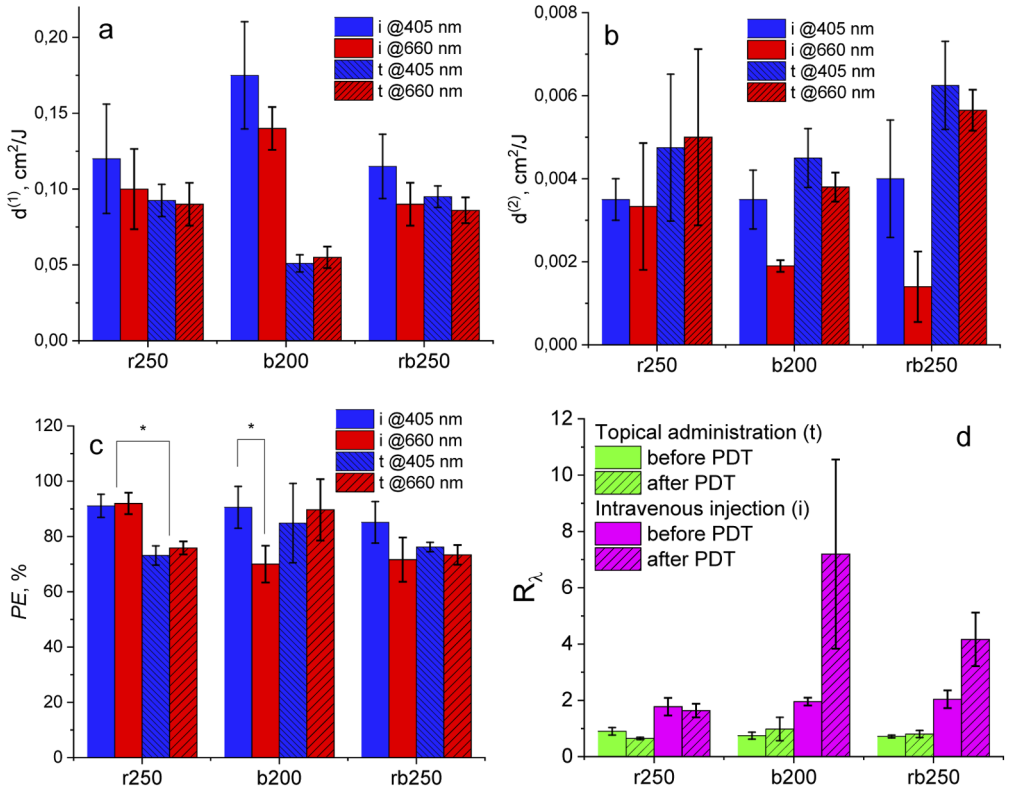

Fig. 4. Photobleaching rate constants $d^{(1)}$ (a) and $d^{(2)}$ (b), photobleaching efficiency *PE* (c) and fluorescence signal ratio R_λ (d) registered upon fluorescence excitation by blue (@405 nm) and red (@660 nm) light in different intravenous (i) and topical application (t) regimes of the PDT procedure according to Table 1. Asterisk shows statistically significant difference.

Typical values of photobleaching efficiency *PE* defined by formula (3) for all the considered PDT regimes are shown in Fig. 4(c). For all cases average *PE* values exceed 70% indicating a high percentage of PS molecules involved into a photodynamic reaction in the probing volume. Monitoring of PDT_r250-i procedure demonstrates high *PE* at both probing wavelengths owing to efficient penetration of red light into tumor tissue where PS is primarily accumulated. In the case of PDT_r250-t *PE* is smaller presumably owing to shorter interval of "fast" kinetics as

Biomedical Optics EXPRESS

compared to PDT_r250-i. In the PDT_b200-i regime with intravenous PS delivery, a statistically significant difference at red and blue excitation wavelengths is observed due to the dominating superficial exposure. PDT_b200-t regime demonstrates high *PE* owing to efficient absorption of blue light by the PS accumulated in superficial layers, revealing no significant difference between two excitation wavelengths. Dual-wavelength regime with intravenous injection demonstrates smaller *PE* as compared to PDT_r250-i and smaller difference between the excitation wavelengths as compared to PDT_b200-i. PDT_rb250-t regime shows the values close to the corresponding red light regime. Note that high *PE* values in the case of topical administration regimes indicate only efficient impact in the superficial tumor layers, while the tumor response can be weak due to absence of PS in deeper tumor layers. In this situation, the ratio of fluorescence signals at the two excitation wavelengths, R_λ, which correlates with the PS accumulation depth [42] may serve as an additional predictive factor of PDT efficacy.

As it was shown by modelling, the value of R_λ characterizes in-depth distribution of PS, and the increase in this value indicates the increase in the relative PS content at higher depths. The values of R_λ in tumor ROI calculated before and after PDT procedure are shown in Fig. 4(d). For topical application the values of R_λ are smaller ($R_\lambda \sim 1$) as compared to those for intravenous injection ($R_\lambda \sim 2$), since the PS localization depth is higher in the latter case, which is in agreement with the simulation predictions [42]. Quantitative depth estimations require further studies for particular parameters, however, qualitative analysis is applicable. Analysis of R_λ provides an additional information regarding PDT procedure: if the value of R_λ is preserved after the procedure, the photobleaching in the tissue can be treated as more uniform, while significant alteration in R_λ indicates a non-uniform photobleaching. A significant increase in R_λ ($R_\lambda \sim 5$) as a result of blue light procedure with intravenous injection (PDT_b200-i) is explained by dominant superficial photobleaching, while red light procedure (PDT_r250-i) demonstrates the preservation of the R_λ value; dual-wavelength regime (PDT_rb250-i) demonstrates smaller alteration as compared to PDT_b200-i, indicating the non-uniformity that was provided by the blue light part. Topical application regimes do not reveal any significant alterations as a result of the procedure, allowing to assume that PS penetration depth is smaller or comparable to the light penetration depth at both irradiation wavelengths. Thus, monitoring of R_λ provides an additional tool for analysis of PDT impact depth.

Tumor temperature in the course of PDT procedure was controlled by an IR-thermometer. To avoid tumor overheating during PDT, the light exposure was interrupted when the temperature reached 42°C to provide heat relaxation. Prior to the procedure the average temperature in tumor located on the mouse leg was 25.6 ± 0.5°C. Temperature increase ΔT as a result of irradiation for

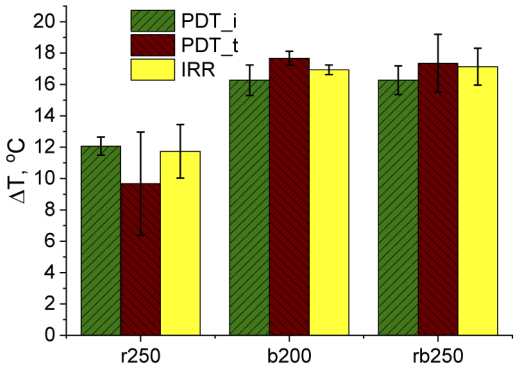

Fig. 5. Temperature increase ΔT as the result of PDT and irradiation for different exposure regimes.

Biomedical Optics EXPRESS

different regimes is shown in Fig. 5(b). Average temperature increase is higher for blue light and dual-wavelength PDT regimes due to higher tissue absorption at 405 nm as compared to 660 nm, and the regimes with red light irradiation induce reliably smaller temperature increase ($p<0.02$). No statistically significant difference in the temperature increase between PDT regimes (both intravenous and topical application) and corresponding IRR regimes was revealed.

3.2. PDT procedures outcomes

Red light PDT is a traditional approach for chlorin based PSs [54–56,69,70]. Panels of images of tumor growth dynamics for red light exposure regimes ($\lambda = 660$ nm) are shown in Fig. 6. This figure shows the images of an untreated tumor, tumor after red light exposure without PS application (IRR_r250), and tumors undergone red light PDT protocol after topical administration (PDT_r250-t) and intravenous injection (PDT_r250-i) prior to (Fig. 6(a)), immediately after (Fig. 6(b)), in 1 (Fig. 6(c)), 4 (Fig. 6(d)), and 7 (Fig. 6(e)) days after exposure. The most pronounced visual tumor degradation is achieved from the intravenous injection protocol.

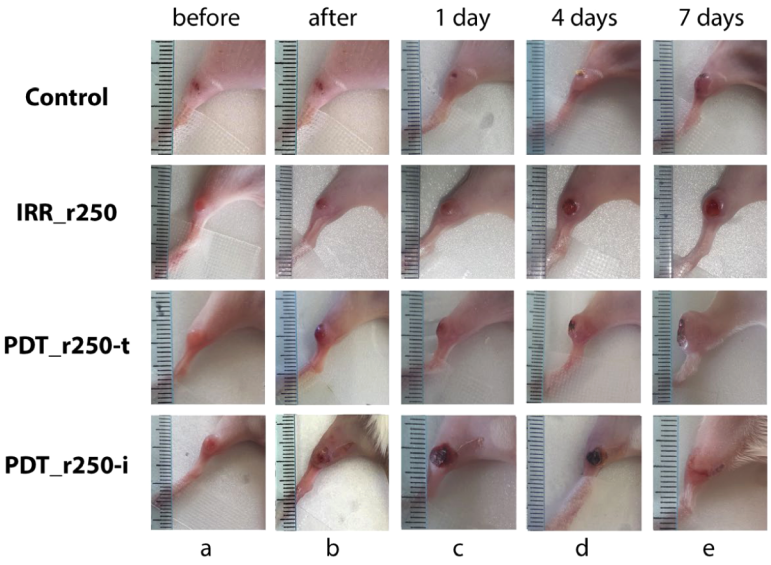

Fig. 6. Photos of an untreated tumor, tumor after red light exposure without PS application (IRR_r250), and tumors undergone red light PDT protocol after topical administration (PDT_r250-t) and intravenous injection (PDT_r250-i) prior to (a), immediately after (b), in 1 (c), 4 (d), and 7 (e) days after exposure at $\lambda = 660$ nm with the light dose of 250 J/cm^2. Millimeter scale is given for reference.

Generalized data on tumor volume progression for different animal groups with topical PS application (PDT-t) is shown in Fig. 7(a). Corresponding dynamics for tumor natural growth (control) and irradiation only (IRR) groups are given as a reference. The most significant suppression of tumor growth is observed for the PDT_b200-t group. Note that the treatment efficiency partially correlates with the *PE* value, which is the highest for PDT_b200-t regime among all topical application regimes. It is worth mentioning that the groups PDT_r250-t and PDT_rb250-t do not demonstrate a significant difference from the corresponding IRR groups though their *PE* values are above 70%. Moreover, although the tumor growth is suppressed or slowed down in the groups with red light regimes during the first three days after the procedure in comparison with the control group, in 7 days these tumors have the same average size as in the control group.

Biomedical Optics EXPRESS

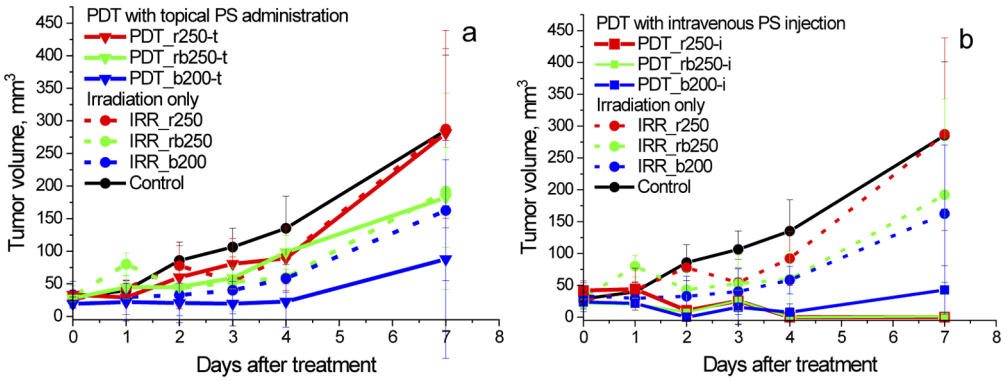

Fig. 7. Tumor growth dynamics after PDT procedures with topical PS administration (a) and intravenous PS injection (b) for red (r) and blue (b) light procedures and combined action (rb). Untreated (control) tumor growth dynamics and the results for irradiation without PS administration are given for reference.

Results of tumor progression monitoring for the protocols with intravenous PS injection (PDT-i) are shown in Fig. 7(b). Both PDT_r250-i and PDT_rb250-i protocols provide positive outcome manifested by full suppression of tumor development observed in 5 days after the procedure. Blue light protocol (PDT_b200-i) also yields tumor growth suppression, however, in one animal the tumor disappearance was incomplete. This can be associated with smaller penetration depth of the blue light and therefore, insufficient light dose delivered to the full thickness of the tumor due to high superficial absorption. In accordance with visual inspection, a total of full responder animals for the regimes with intravenous injection was 8 out of 9 animals in three PDT-i groups.

It is worth mentioning that both red light and dual-wavelength regimes demonstrate significant difference depending on the PS application mode: topical application groups (PDT_r250-t and PDT_rb250-t) demonstrate weak response manifested by initial suppression of tumor growth followed by further tumor progression, while intravenous injection groups (PDT_r250-i and PDT_rb250-i) demonstrate full response in all animals. On the contrary, the difference between blue light regimes is weaker: PDT_b200-t regime demonstrates the strongest tumor growth suppression among all PDT-t regimes, while PDT_b200-i includes only one non-responder. The results are in line with the results of fluorescence monitoring: the intravenous regimes with deeper PS accumulation demonstrated better response than topical application regimes. The blue light intravenous regime, for which the demonstrated alteration of R_λ as a results of PDT procedure was maximal, demonstrated weaker efficacy as compared to red light and dual-wavelength regimes, for which the alteration was smaller. It is worth mentioning that non-contact temperature monitoring demonstrates higher temperature increase (up to 42°C) during exposure by blue light and in dual-wavelength regime in comparison to red light. In this connection, the observed effect can be explained by a combined effect of PDT and hyperthermia with presumable prevalence of the latter mechanism.

In order to quantify the effect of different exposures to tumors, we calculated the tumor growth inhibition factor TGI according to Eq. (2) for the averaged values of tumor size in each animal group in 4 and 7 days after the treatment. The results are summarized in Fig. 8. All the protocols with intravenous PS injection demonstrate about 80% suppression of tumor growth in 4 days after the treatment. Among all PS topical application groups only blue light regime (PDT_b200-t) demonstrates a comparable effect, while for the two other color schemes it is less pronounced (25 and 45% for PDT_r250-t and PDT_rb250-t, respectively). The irradiation only regimes demonstrate TGI in the range of 49-62% for all three groups. The situation changes

Biomedical Optics EXPRESS

quite dramatically in 7 days after the exposure: for red light and dual wavelength exposures with intravenous injection TGI reaches 100% together with 85% for blue light exposure caused by a single animal with no full response in PDT_b200-i group. Both other red light regimes (IRR_r250 and PDT_r250-t) demonstrate zero TGI indicating that tumor reaches the size comparable to that for the control group, allowing to assume that in the view of the preserved effect in 4 days, additional procedures are recommended for these cases. Blue light exposure demonstrates highest TGI values in 7 days among both irradiation only and topical application protocols (43 and 70% for IRR_b200 and PDT_b200-t, respectively), although, they are lower than those in 4 days. The trend for the TGI decrease in 7 days is also observed for dual-wavelength exposure for both irradiation only and topical application protocols, which may also serve as an indicator for the treatment protocol correction requirement.

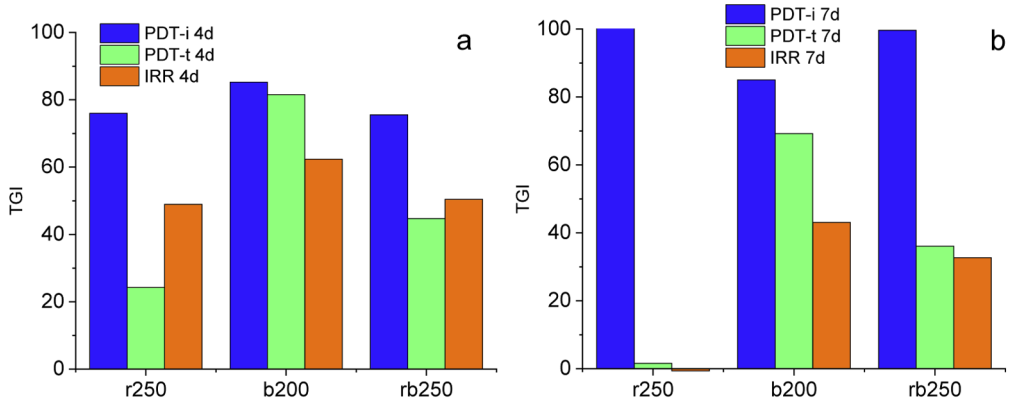

Fig. 8. Tumor growth inhibition factor (TGI) for different treatment regimes in 4 (a) and 7 (b) days after the procedure.

3.3. OCT angiography

Results of OCT-A monitoring during 7 days since the procedure for the four groups (PDT_r250-t, PDT_r250-i, IRR_r250, Control) are shown in Fig. 9. The images were acquired from the center of the tumor, while the linear size of the tumor exceeded the linear size of the field of view, thus, the entire imaging area corresponds to the tumor. Angiographic OCT images of tumors prior to the exposure demonstrate typical microvasculature of tumor itself and tumor-supporting vessels in superficial skin layers. These vessels have typical wavy shape and relatively large density. Since OCT-A approach is based on the speckle correlation measurement [60], it maps only vessels with active blood flow, while disappearance of vessels in OCT-A images indicates interruption in microcirculatory activity and can serve as a positive prognostic factor of the tumor response to the treatment [49,50]. Figure 9 demonstrates that total disappearance of the vessels is observed only in PDT_r250-i group (bottom line), while for both control group and topical administration protocol PDT_r250-t the microcirculatory activity is preserved.

Since typical time to observe the effect of microcirculation obliteration with OCT-A as a result of PDT is 24 hours [49,50], OCT-A data in 1 day after exposure were analyzed and summarized in Table 3 for all studied protocols. The number of occurrences of microcirculation interruption similar to that acquired for the PDT_r250-i was calculated in each group. The values (N_r/N_t) indicate the number of animals with complete microcirculation interruption (N_r) in accordance to OCT-A out of total number of animals in the group (N_t). All the intravenous injection regimes demonstrate tumor response manifested by microcirculatory activity suppression in all animals 24 hours after the procedure. Among other regimes, only blue light exposures, both PDT_b200-t

Biomedical Optics EXPRESS

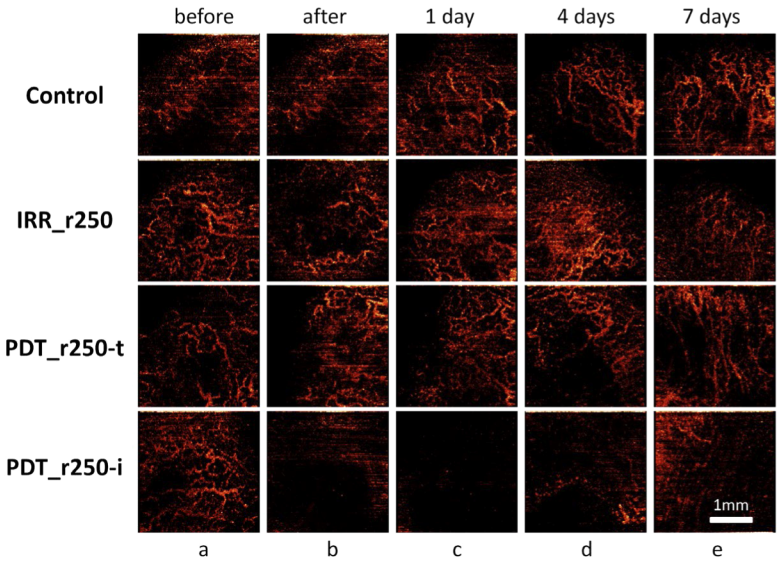

Fig. 9. Results of angiographic OCT monitoring of natural tumor growth (Control), tumor after IRR_r250 exposure without PS administration, after PDT with PS topical administration (PDT_r250-t) and intravenous injection (PDT_r250-i) at $\lambda = 660$ nm with dose of 250 J/cm^2 prior to (a), immediately after (b), in 1(c), 4(d), and 7(e) days after exposure. The bottom row corresponding to PDT_r250-i protocol demonstrates the interruption of tumor microcirculatory activity observed by OCT-angiography.

and IRR_b200, demonstrate tumor response to the treatment in most animals manifested by disappearance of the tumor vasculature in OCT-A images. Only one animal had microcirculation interruption in PDT_rb250-t group.

Table 3. Microcirculation interruption in tumor as a result of exposure observed by OCT angiography for different animal groups (microcirculation interruption occurrences/total number of animals in a group)

Treatment protocol	Exposure regime		
	r250	b200	rb250
PDT-i	3/3	3/3	3/3
PDT-t	0/3	3/3	1/3
IRR	0/3	2/3	0/3
Control	0/5		

The results of OCT monitoring are in good agreement with the results of visual inspection, which revealed that full tumor response to treatment is observed primarily for the intravenous injection protocols. The observed results are also in line with the results of other papers on OCT monitoring of PDT protocols with intravenous PS injection [49,50]. It is worth mentioning that since the probing depth of OCT-A is limited by 1 mm, only microcirculation interruption in superficial tumor tissues can be revealed with this technique, while underlying tumor layers may preserve blood supply. This explains a non-responder in PDT_b200-i group for which the OCT-A indicated microcirculation interruption and is in line with results reported in paper [50], which demonstrated superficial tumor necrosis with underlying viable tumor in a non-responder after PDT with intravenous injection. The most pronounced response in irradiation only and topical application groups provided by the blue light regimes is consistent with the results of our

Biomedical Optics EXPRESS

previous study on normal tissues [13]. Note that OCT monitoring results do not demonstrate any difference between different intravenous injection groups, on the contrary to dual-wavelength FI results which revealed difference in R_λ alteration as a result of PDT procedure.

3.4. Histology study

Histological images of tumor tissue for different animal groups are shown in Fig. 10. Table 4 summarizes typical features revealed by histology examination for all the considered groups together with the tumor response scores. Histological studies demonstrated that no alterations or weak alterations in tumorous cells morphology were revealed in the control untreated group (Grade 1), in IRR_r250 and IRR_rb250 group in 7 days after the treatment (Grade 2 and 1, respectively). It is worth mentioning that even in the case of natural growth the employed tumor model may exhibit necrotic cells in the tumor core due to weakened blood supply in the tumor center caused by fast tumor development (spontaneous necrosis). Despite the absence of complete tumor response to PDT procedures with topical PS application, histological studies revealed morphological alterations for these treatment regimes. PDT_r250-t and PDT_rb250-t groups demonstrate Grade 2 tumor response corresponding to weak alterations, although local necrosis foci are revealed for these groups. Both blue light regimes with irradiation only and topical application of PS demonstrate higher tumor response grade (Grade 2 and 3 for IRR_b200 and PDT_b200-t, respectively) as compared to red light and dual-wavelength exposure, which may be associated with partial hyperthermia effect.

On the contrary, PDT_b200-i group demonstrates the lowest response score from all intravenous injection groups (Grade 3 for PDT_b200-i versus Grade 4 for PDT_r250-i and PDT_rb250-i), although it exceeds all scores for control, irradiation only and topical application groups, except for PDT_b200-t regime with the same Grade 3. PDT_r250-i and PDT_rb250-i groups demonstrate the best tumor response scores (Grade 4) in all animals. It is worth mentioning that PDT regimes with intravenous injection demonstrate vessel destruction occurrences in histological analysis confirming vascular mechanism of PDT with chlorin-based PS. Essential morphological alterations not observed in the control group and serving as the indicators of tumor response to treatment include active proliferation of connective tissues, pathological mitosis, appearance of giant cells and hyalinosis. Increase of mitotic activity may serve as the initial sign of tumor reaction to the exposure, while appearance of cells with pathologic mitosis and giant cells indicate significant morphologic alterations with high probability of further full tumor response. The results of histological analysis are in line with both *in vivo* OCT observations and tumor growth monitoring. OCT observations reveal interruption in the tumor microcirculation for PDT_r250-i and PDT_rb250-i groups. The same groups demonstrate strongest response to treatment in accordance with the tumor size monitoring and show no observable tumor in 7 days after treatment, which agrees with the highest tumor response score derived from the histological analysis.

Concerning blue light regimes, both irradiation only (IRR_b200) and topical application (PDT_b200-t) regimes demonstrate better tumor growth suppression than corresponding red light and dual-wavelength regimes. This is in agreement with morphological studies which show significant tumor response score in these groups. This effect, on the one hand, may be associated with additional hyperthermia of the tumor, since the absorption of blue light in tissues is stronger than of red light. On the other hand, it is worth mentioning that typical temperature increase values are comparable for the blue light and dual wavelength regimes, although the total dose of the light absorbed in the superficial tumor layers is higher for the blue light regimes.

Biomedical Optics EXPRESS

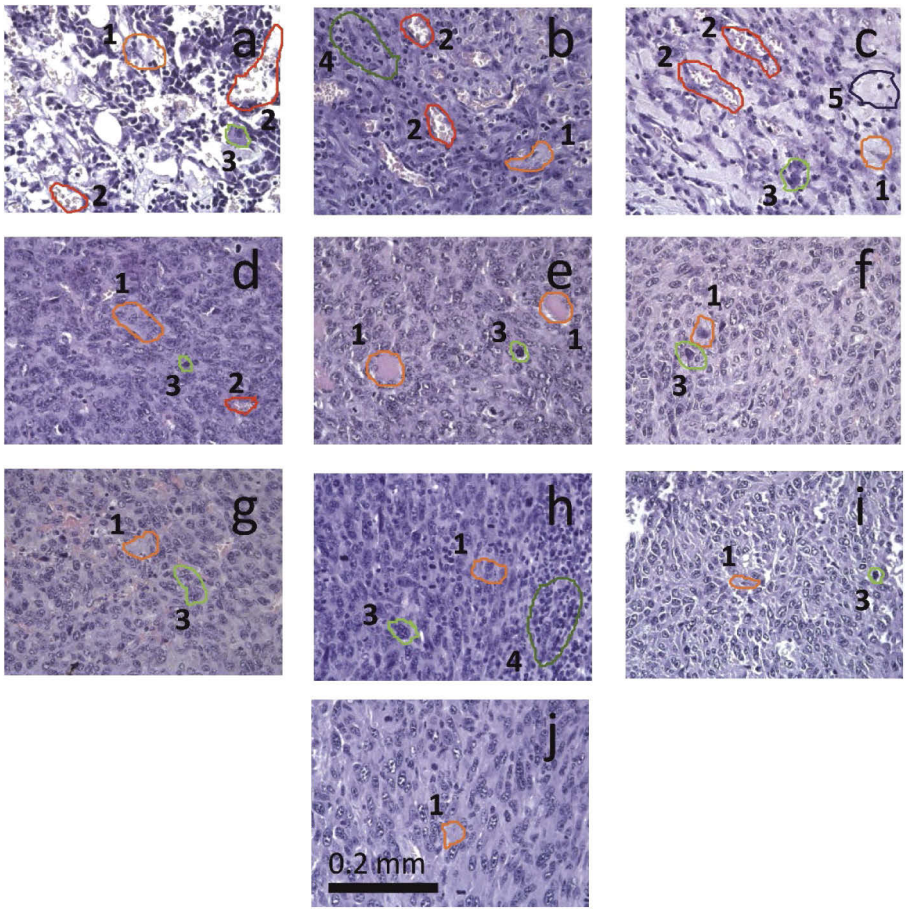

Fig. 10. Histological images of tumors in 7 days after red light exposure (a - PDT_r250-i, d - PDT_r250-t, g - IRR_r250), blue light exposure (b - PDT_b200-i, e - PDT_ b200-t, h - IRR_b200), dual-wavelength exposure (c - PDT_rb250-i, f - PDT_rb250-t, i - IRR_rb250), and an untreated tumor (j). Typical observed changes are outlined in the figures: (1) dystrophic cell alterations and necrobiosis, (2) vessel destruction, (3) increased mitotic activity and formation of giant cells, (4) inflammatory infiltration, (5) hyalinosis of tumor stroma.

Biomedical Optics EXPRESS

Table 4. Tumor response scores for different animal groups derived from histologic studies

Treatment protocol	Exposure regime		
	r250	b200	rb250
PDT-i	Grade 4. Destruction of tumor tissue with the presence of massive necrosis. Full elimination of tumor blood vessels in a single sample. Proliferation of connective tissue, hialynosis. Partially preserved tumor tissue with excessive presence of pathologic mitoses and giant cells.	Grade 3. Absence of typical tumor morphology as a result of massive necrosis, pronounced microcirculation disorders, and proliferation of connective tissue. Inflammatory reaction manifested by round-shaped cells. Increase in mitotic activity with the presence of pathologic mitoses and giant cells.	Grade 4. Massive necrosis with areas of full elimination of tumor tissue. Proliferation of connective tissue both at the periphery and in the tumor center, hialynosis. Partially preserved tumor tissue with the excessive presence of pathologic mitoses and giant cells.
PDT-t	Grade 2. Areas of unaltered tumor tissue, partial dystrophic and necrobiotic alterations of tumor cells. Alterations in tumor stroma manifested by microcirculation disorders, hemorrhages, focal proliferation of connective tissue, and focal increase of mitotic activity.	Grade 3. Absence of typical tumor morphology as a result of massive necrosis, pronounced microcirculation disorders, and proliferation of connective tissue. Pronounced inflammatory reaction. Increase in mitotic activity with the presence of pathologic mitoses and giant cells.	Grade 2. Areas of unaltered tumor tissue, partial dystrophic and necrobiotic alterations of tumor cells. Alterations in tumor stroma manifested by microcirculation disorders, hemorrhages, focal proliferation of connective tissue, and focal increase of mitotic activity.
IRR	Grade 2. Areas of unaltered tumor tissue, partial dystrophic and necrobiotic alterations of tumor cells. Alterations in tumor stroma manifested by microcirculation disorders, hemorrhages, focal proliferation of connective tissue, and focal increase of mitotic activity.	Grade 2. Destruction of typical tumor structure due to cells dystrophic alterations, focal necrosis and focal proliferation of connective tissues. Weak manifestation of inflammatory reaction by round-shaped cells infiltration. Increase in mitotic activity with the presence of pathologic mitoses and giant cells.	Grade 1. Primarily unaltered tumor tissue, partial dystrophic and necrobiotic alterations of tumor cells. Alterations in tumor stroma manifested by microcirculation disorders, hemorrhages, focal proliferation of connective tissue, and focal increase of mitotic activity.
CONTROL	Grade 1. Primarily unaltered tumor tissue, partial dystrophic and necrobiotic alterations of tumor cells. Alterations in tumor stroma manifested by hemorrhages, focal proliferation of connective tissue, and focal increase of mitotic activity.		

Biomedical Optics EXPRESS

4. Conclusion

A comparative study of red and blue light PDT regimes with topical application and intravenous injection of PS was performed in laboratory mice *in vivo*. Fluorescence imaging allowed to trace the PS accumulation and its photobleaching as a result of a PDT procedure. The photobleaching kinetics was demonstrated to be well fitted by a bi-exponential curve with the "fast" rate constant exceeding the "slow" one for about an order of magnitude. The difference in the observed kinetics is determined by different distribution of PS within tissue depending on the way of PS administration, different in-depth distribution of red-light and blue-light irradiance, and different FI probing volume depending on the fluorescence excitation wavelength. Dual-wavelength FI modality allowed to reveal the difference in typical procedure impact depth for intravenous PS injection based on the fluorescence signal ratio. Photobleaching efficiency averaged over the animal group varied between 70 and 90%.

Analysis of the tumor progression after treatment demonstrated that all the considered PDT regimes suppress tumor growth. However, for red light exposure with topical PS application and the irradiation only regime, the tumor size reaches that for the control group in 7 days after the treatment. Dual-wavelength regime shows partial suppression of tumor in relation to the control group, while blue light regime provides the most pronounced effect among both PS topical application and irradiation only groups. Relatively low response of tumors to PDT with topical PS administration presumably originates from weak accumulation of PS in deeper tissues. Observations in groups with intravenous PS injection demonstrate opposite trends: red light and dual-wavelength regimes provide good tumor response and treatment outcome, while the blue light group contains a non-responder. This effect may be associated with low penetration depth of blue light, which may prevent delivery of the necessary light dose to deeper tumor layers and was confirmed by dual-wavelength FI observations. The results of tumor growth analysis are in line with OCT-A observations: the animals with high tumor growth suppression demonstrated interruption in microcirculatory activity in tumor according to OCT-angiography data, while tumors with low response demonstrated preservation of microcirculation after the procedure.

The results of histology study also correlate with the tumor development observations. Red light and dual-wavelength regimes of PDT with intravenous PS injection demonstrate the highest grades of tumor response in accordance with morphology analysis. Observed effects include tumor cell necrosis, pathological mitosis, hemorrhage, and destruction of vessel walls. Blue light PDT group with intravenous injection demonstrates weaker response with a possibility for further tumor progression in one case. On the contrary, the most significant morphological alterations in groups of PDT with topical application and irradiation only are observed for blue light. Control group also demonstrates particular pathological alterations due to fast tumor development that leads to spontaneous necrosis.

The employed approach of PDT optical monitoring *in vivo* including newly introduced dual-wavelength FI and OCT-A allowed to reveal peculiarities in PDT performance with different ways of PS administration and different irradiation wavelengths thus showing its potential for further extensive use in various PDT applications.

Funding. Russian Science Foundation (17-15-01264).

Acknowledgements. The authors are grateful to Dr. I. Turchin for useful discussions, to K. Pavlova, Yu. Ivanova, N. Markina, Dr. A. Volovetsky, Dr. N. Shilyagina, Dr. I. Balalaeva, and Dr. A. Brilkina for assistance in animal handling and management, to Dr. V. Perekatova for her help in manuscript preparation.

Disclosures. The authors have declared that no competing interest exists.

References

1. S. Mallidi, S. Anbil, A.-L. Bulin, G. Obaid, M. Ichikawa, and T. Hasan, "Beyond the barriers of light penetration: strategies, perspectives and possibilities for photodynamic therapy," Theranostics **6**(13), 2458–2487 (2016).
2. S. Marchal, G. Dolivet, H.-P. Lassalle, F. Guillemin, and L. Bezdetnaya, "Targeted photodynamic therapy in head and neck squamous cell carcinoma: heading into the future," Lasers Med. Sci. **30**(9), 2381–2387 (2015).

Biomedical Optics EXPRESS

3. M. H. E. Jansen, F. H. J. Koekelkoren, P. J. Nelemans, A. Arits, M. H. Roozeboom, N. W. J. Kelleners-Smeets, and K. Mosterd, "Comparison of long-term cosmetic outcomes for different treatments of superficial basal cell carcinoma," J. Am. Acad. Dermatol. **79**(5), 961–964 (2018).
4. K. Svanberg, T. Andersson, D. Killander, I. Wang, U. Stenram, S. Andersson-Engels, R. Berg, J. Johansson, and S. Svanberg, "Photodynamic therapy of non-melanoma malignant tumours of the skin using topical delta-amino levulinic acid sensitization and laser irradiation," Br. J. Dermatol. **130**(6), 743–751 (1994).
5. S. M. Banerjee, S. El-Sheikh, A. Malhotra, C. A. Mosse, S. Parker, N. R. Williams, A. J. MacRobert, R. Hamoudi, S. G. Bown, and M. R. S. Keshtgar, "Photodynamic therapy in primary breast cancer," J. Clin. Med. **9**(2), 483 (2020).
6. D. Zaak, R. Sroka, M. Höppner, W. Khoder, O. Reich, S. Tritschler, R. Muschter, R. Knüchel, and A. Hofstetter, "Photodynamic Therapy by Means of 5-ALA induced PPIX in human prostate cancer – preliminary results," Med. Laser Appl. **18**(1), 91–95 (2003).
7. S. G. Bown, A. Z. Rogowska, D. E. Whitelaw, W. R. Lees, L. B. Lovat, P. Ripley, L. Jones, P. Wyld, A. Gillams, and A. W. Hatfield, "Photodynamic therapy for cancer of the pancreas," Gut **50**(4), 549–557 (2002).
8. B. C. Wilson and M. S. Patterson, "The physics, biophysics and technology of photodynamic therapy," Phys. Med. Biol. **53**(9), R61–R109 (2008).
9. D. Straten, V. Mashayekhi, H. S. de Bruijn, S. Oliveira, and D. J. Robinson, "Oncologic photodynamic therapy: basic principles, current clinical status and future directions," Cancers **9**(12), 19 (2017).
10. P. Agostinis, K. Berg, K. A. C. Thomas, H. Foster, A. W. Girotti, S. O. Gollnick, S. M. Hahn, M. R. Hamblin, A. Juzeniene, D. Kessel, M. Korbelik, J. Moan, P. Mroz, D. Nowis, J. Piette, B. C. Wilson, and J. Golab, "Photodynamic therapy of cancer: an update," Ca-Cancer J. Clin. **61**(4), 250–281 (2011).
11. V. V. Tuchin, *Tissue Optics: Light Scattering Methods and Instruments for Medical Diagnostics*, 4th ed. (SPIE Press, 2015).
12. M. Shakhova, D. Loginova, A. Meller, D. Sapunov, N. Orlinskaya, A. Shakhov, A. Khilov, and M. Kirillin, "Photodynamic therapy with chlorin-based photosensitizer at 405 nm: numerical, morphological, and clinical study," J. Biomed. Opt. **23**(09), 1 (2018).
13. D. Kurakina, A. Khilov, M. Shakhova, N. Orlinskaya, E. Sergeeva, A. Meller, I. Turchin, and M. Kirillin, "Comparative analysis of single- and dual-wavelength photodynamic therapy regimes with chlorin-based photosensitizers: animal study," J. Biomed. Opt. **25**(06), 1 (2020).
14. G. Greening, A. Mundo, N. Rajaram, and T. J. Muldoon, "Sampling depth of a diffuse reflectance spectroscopy probe for in-vivo physiological quantification of murine subcutaneous tumor allografts," J. Biomed. Opt. **23**(08), 1 (2018).
15. L. Helander, H. E. Krokan, A. Johnsson, O. A. Gederaas, and K. Plaetzer, "Red versus blue light illumination in hexyl 5-aminolevulinate photodynamic therapy: the influence of light color and irradiance on the treatment outcome in vitro," J. Biomed. Opt. **19**(8), 088002 (2014).
16. Z. Jamali, S. M. Hejazi, S. M. Ebrahimi, H. Moradi-Sardareh, and M. Paknejad, "Effects of LED-Based photodynamic therapy using red and blue lights, with natural hydrophobic photosensitizers on human glioma cell line," Photodiagn. Photodyn. Ther. **21**, 50–54 (2018).
17. H. Masuda, M. Kimura, A. Nishioka, H. Kato, and A. Morita, "Dual wavelength 5-aminolevulinic acid photodynamic therapy using a novel flexible light-emitting diode unit," J. Dermatol. Sci. **93**(2), 109–115 (2019).
18. T. Hatakeyama, Y. Murayama, S. Komatsu, A. Shiozaki, Y. Kuriu, H. Ikoma, M. Nakanishi, D. Ichikawa, H. Fujiwara, K. Okamoto, T. Ochiai, Y. Kokuba, K. Inoue, M. Nakajima, and E. Otsuji, "Efficacy of 5-aminolevulinic acid-mediated photodynamic therapy using light-emitting diodes in human colon cancer cells," Oncol. Rep. **29**(3), 911–916 (2013).
19. H. Hino, Y. Murayama, M. Nakanishi, K. Inoue, M. Nakajima, and E. Otsuji, "5-Aminolevulinic acid-mediated photodynamic therapy using light-emitting diodes of different wavelengths in a mouse model of peritoneally disseminated gastric cancer," J. Surg. Res. **185**(1), 119–126 (2013).
20. M. M. Tsoukas, S. González, T. J. Flotte, R. R. Anderson, M. E. Sherwood, and N. Kollias, "Wavelength and fluence effect on vascular damage with photodynamic therapy on skin," J. Invest. Dermatol. **114**(2), 303–308 (2000).
21. F. Mougel, S. Debarbieux, S. Ronger-Savle, S. Dalle, and L. Thomas, "Methylaminolaevulinate photodynamic therapy in patients with multiple basal cell carcinomas in the setting of Gorlin-Goltz syndrome or after radiotherapy," Dermatology **219**(2), 138–142 (2009).
22. A. Itkin and B. A. Gilchrest, "delta-Aminolevulinic acid and blue light photodynamic therapy for treatment of multiple basal cell carcinomas in two patients with nevoid basal cell carcinoma syndrome," Dermatol. Surg. **30**, 1054–1061 (2004).
23. E. V. Maytin, U. Kaw, M. Ilyas, J. A. Mack, and B. Hu, "Blue light versus red light for photodynamic therapy of basal cell carcinoma in patients with Gorlin syndrome: A bilaterally controlled comparison study," Photodiagn. Photodyn. Ther. **22**, 7–13 (2018).
24. C. A. Morton, C. Whitehurst, J. V. Moore, and R. M. Mackie, "Comparison of red and green light in the treatment of Bowen's disease by photodynamic therapy," Br. J. Dermatol. **143**(4), 767–772 (2000).
25. G. Garcia de Carvalho, J. C. Sanchez-Puetate, M. C. Donatoni, P. M. M. Huacho, A. N. de Souza Rastelli, K. T. de Oliveira, D. M. Palomari Spolidorio, and D. L. Zandim-Barcelos, "Photodynamic inactivation using a chlorin-based photosensitizer with blue or red-light irradiation against single-species biofilms related to periodontitis," Photodiagn. Photodyn. Ther. **31**, 101916 (2020).

Biomedical Optics EXPRESS

26. M. Kim, H. Y. Jung, and H. J. Park, "Topical PDT in the treatment of benign skin diseases: principles and new applications," Int. J. Mol. Sci. **16**(10), 23259–23278 (2015).
27. C. Cantisani, G. Paolino, V. Faina, F. Frascani, F. Cantoresi, D. Bianchini, and S. Calvieri, "Overview on Topical 5-ALA photodynamic therapy use for non melanoma skin cancers," Int. J. Photoenergy **2014**, 1–7 (2014).
28. M. Fadel, K. Kassab, D. A. Abdel Fadeel, and M. A. Farag, "Topical photodynamic therapy of tumor bearing mice with meso-tetrakis (N-methyl-4-pyridyl) porphyrin loaded in ethosomes," Photodiagn. Photodyn. Ther. **30**, 101789 (2020).
29. J. P. Celli, B. Q. Spring, I. Rizvi, C. L. Evans, K. S. Samkoe, S. Verma, B. W. Pogue, and T. Hasan, "Imaging and photodynamic therapy: mechanisms, monitoring, and optimization," Chem. Rev. **110**(5), 2795–2838 (2010).
30. L. B. Josefsen and R. W. Boyle, "Unique diagnostic and therapeutic roles of porphyrins and phthalocyanines in photodynamic therapy, imaging and theranostics," Theranostics **2**(9), 916–966 (2012).
31. K. R. Rollakanti, S. C. Kanick, S. C. Davis, B. W. Pogue, and E. V. Maytin, "Techniques for fluorescence detection of protoporphyrin IX in skin cancers associated with photodynamic therapy," Photonics Lasers Med. **2**(4), 287–303 (2013).
32. A. Johansson, F. Faber, G. Kniebühler, H. Stepp, R. Sroka, R. Egensperger, W. Beyer, and F. W. Kreth, "Protoporphyrin IX fluorescence and photobleaching during interstitial photodynamic therapy of malignant gliomas for early treatment prognosis," Lasers Surg. Med. **45**(4), 225–234 (2013).
33. M. Scott, C. Hopper, A. Sahota, R. Springett, B. McIlroy, S. Bown, and A. MacRobert, "Fluorescence photodiagnostics and photobleaching studies of cancerous lesions using ratio imaging and spectroscopic techniques," Lasers Med. Sci. **15**(1), 63–72 (2000).
34. D. Kurakina, V. Perekatova, V. Plekhanov, A. Orlova, E. Sergeeva, A. Khilov, A. Nerush, P. Subochev, S. Mallidi, I. Turchin, and T. Hasan, "Towards bimodal optical monitoring of photodynamic therapy with targeted nanoconstructs: a phantom study," Appl. Sci. **9**(9), 1918 (2019).
35. J. Tyrrell, S. Campbell, and A. Curnow, "Protoporphyrin IX photobleaching during the light irradiation phase of standard dermatological methyl-aminolevulinate photodynamic therapy," Photodiagn. Photodyn. Ther. **7**(4), 232–238 (2010).
36. M. T. Jarvi, M. S. Patterson, and B. C. Wilson, "Insights into photodynamic therapy dosimetry: simultaneous singlet oxygen luminescence and photosensitizer photobleaching measurements," Biophys. J. **102**(3), 661–671 (2012).
37. S. Anbil, I. Rizvi, J. P. Celli, N. Alagic, and T. Hasan, "A photobleaching-based PDT dose metric predicts PDT efficacy over certain BPD concentration ranges in a three-dimensional model of ovarian cancer," Proc. SPIE **8568**, 85680S (2013).
38. S. Mallidi, B. Q. Spring, and T. Hasan, "Optical imaging, photodynamic therapy and optically triggered combination treatments," Cancer J. (Philadelphia, PA, U. S.) **21**(3), 194–205 (2015).
39. S. Gamayunov, I. Turchin, I. Fiks, K. Korchagina, M. Kleshnin, and N. Shakhova, "Fluorescence imaging for photodynamic therapy of non-melanoma skin malignancies— a retrospective clinical study," Photonics Lasers Med. **5**(2), 101–111 (2016).
40. A. Khilov, D. Loginova, E. Sergeeva, M. Shakhova, A. Meller, I. Turchin, and M. Kirillin, "Two-wavelength fluorescence monitoring and planning of photodynamic therapy," Sovrem Tekhnologii Med. **9**(4), 96–105 (2017).
41. A. V. Khilov, M. Y. Kirillin, D. A. Loginova, and I. V. Turchin, "Estimation of chlorin-based photosensitizer penetration depth prior to photodynamic therapy procedure with dual-wavelength fluorescence imaging," Laser Phys. Lett. **15**(12), 126202 (2018).
42. A. V. Khilov, D. A. Kurakina, I. V. Turchin, and M. Y. Kirillin, "Monitoring of chlorin-based photosensitiser localisation with dual-wavelength fluorescence imaging: numerical simulations," Quantum Electron. **49**(1), 63–69 (2019).
43. S. M. Daly and M. J. Leahy, "'Go with the flow ': a review of methods and advancements in blood flow imaging," J. Biophotonics **6**(3), 217–255 (2013).
44. G. Yu, T. Durduran, C. Zhou, H. W. Wang, M. E. Putt, H. M. Saunders, C. M. Sehga, E. Glatstein, A. G. Yodh, and T. M. Busch, "Noninvasive monitoring of murine tumor blood flow during and after photodynamic therapy provides early assessment of therapeutic efficacy," Clin. Cancer Res. **11**(9), 3543–3552 (2005).
45. D. Chen, J. Ren, Y. Wang, B. Li, and Y. Gu, "Intraoperative monitoring of blood perfusion in port wine stains by laser Doppler imaging during vascular targeted photodynamic therapy: A preliminary study," Photodiagn. Photodyn. Ther. **14**, 142–151 (2016).
46. I. Wang, S. Andersson-Engels, G. E. Nilsson, K. Wardell, and K. Svanberg, "Superficial blood flow following photodynamic therapy of malignant non-melanoma skin tumours measured by laser Doppler perfusion imaging," Br. J. Dermatol. **136**, 184–189 (1997).
47. Y. H. Ong, J. Miller, M. Yuan, M. Chandra, M. Khatib, S. A. Vinogradov, M. E. Putt, T. C. Zhu, K. A. Cengel, A. G. Yodh, and T. M. Busch, "Blood flow measurements enable optimization of light delivery for personalized photodynamic therapy," Cancers **12**(6), 1584 (2020).
48. T. L. Becker, A. D. Paquette, K. R. Keymel, B. W. Henderson, and U. Sunar, "Monitoring blood flow responses during topical ALA-PDT," Biomed. Opt. Express **2**(1), 123–130 (2011).
49. M. A. Sirotkina, L. A. Matveev, M. V. Shirmanova, V. Y. Zaitsev, N. L. Buyanova, V. V. Elagin, G. V. Gelikonov, S. S. Kuznetsov, E. B. Kiseleva, A. A. Moiseev, S. V. Gamayunov, E. V. Zagaynova, F. I. Feldchtein, A. Vitkin, and N. D. Gladkova, "Photodynamic therapy monitoring with optical coherence angiography," Sci. Rep. **7**(1), 41506 (2017).

Biomedical Optics EXPRESS

50. M. A. Sirotkina, A. A. Moiseev, L. A. Matveev, V. Y. Zaitsev, V. V. Elagin, S. S. Kuznetsov, G. V. Gelikonov, S. Y. Ksenofontov, E. V. Zagaynova, F. I. Feldchtein, N. D. Gladkova, and A. Vitkin, "Accurate early prediction of tumour response to PDT using optical coherence angiography," Sci. Rep. **9**(1), 6492 (2019).
51. E. V. Gubarkova, F. I. Feldchtein, E. V. Zagaynova, S. V. Gamayunov, M. A. Sirotkina, E. S. Sedova, S. S. Kuznetsov, A. A. Moiseev, L. A. Matveev, V. Y. Zaitsev, D. A. Karashtin, G. V. Gelikonov, L. Pires, A. Vitkin, and N. D. Gladkova, "Optical coherence angiography for pre-treatment assessment and treatment monitoring following photodynamic therapy: a basal cell carcinoma patient study," Sci. Rep. **9**(1), 18670 (2019).
52. M. A. Sirotkina, E. V. Gubarkova, A. A. Plekhanov, A. A. Sovetsky, V. V. Elagin, A. L. Matveyev, L. A. Matveev, S. S. Kuznetsov, E. V. Zagaynova, N. D. Gladkova, and V. Y. Zaitsev, "In vivo assessment of functional and morphological alterations in tumors under treatment using OCT-angiography combined with OCT-elastography," Biomed. Opt. Express **11**(3), 1365–1382 (2020).
53. C. P. Sabino, A. M. Deana, T. M. Yoshimura, D. F. T. da Silva, C. M. França, M. R. Hamblin, and M. S. Ribeiro, "The optical properties of mouse skin in the visible and near infrared spectral regions," J. Photochem. Photobiol., B **160**, 72–78 (2016).
54. T. Trukhachova, "Safety and efficacy of photosensitizer Photolon (Fotolon) in photodynamic therapy," Proc. SPIE **11070**, 1107037 (2019).
55. S. V. Shliakhtsin, T. V. Trukhachova, H. A. Isakau, and Y. P. Istomin, "Pharmacokinetics and biodistribution of Photolon (Fotolon) in intact and tumor-bearing rats," Photodiagn. Photodyn. Ther. **6**(2), 97–104 (2009).
56. Y. P. Istomin, M. A. Kaplan, S. V. Shliakhtsin, T. P. Lapzevich, D. A. Cerkovsky, L. N. Marchanka, A. S. Fedulov, and T. V. Trukhachova, "Immediate and long-term efficacy and safety of photodynamic therapy with Photolon (Fotolon): a seven-year clinical experience," Proc. SPIE **7380**, 73806V (2009).
57. M. S. Kleshnin, I. I. Fiks, V. I. Plekhanov, S. V. Gamayunov, and I. V. Turchin, "Compact and fully automated system for monitoring photodynamic therapy, based on two LEDs and a single CCD," Laser Phys. Lett. **12**(11), 115602 (2015).
58. J. S. Dysart and M. S. Patterson, "Photobleaching kinetics, photoproduct formation, and dose estimation during ALA induced PpIX PDT of MLL cells under well oxygenated and hypoxic conditions," Photochem. Photobiol. Sci. **5**(1), 73–81 (2006).
59. A. D. Tekrony, N. M. Kelly, B. A. Fage, and D. T. Cramb, "Photobleaching kinetics of Verteporfin and Lemuteporfin in cells and optically trapped multilamellar vesicles using two-photon excitation," Photochem. Photobiol. **87**(4), 853–861 (2011).
60. L. A. Matveev, V. Y. Zaitsev, G. V. Gelikonov, A. L. Matveyev, A. A. Moiseev, S. Y. Ksenofontov, V. M. Gelikonov, M. A. Sirotkina, N. D. Gladkova, V. Demidov, and A. Vitkin, "Hybrid M-mode-like OCT imaging of three-dimensional microvasculature in vivo using reference-free processing of complex valued B-scans," Opt. Lett. **40**(7), 1472–1475 (2015).
61. A. Moiseev, S. Ksenofontov, M. Sirotkina, E. Kiseleva, M. Gorozhantseva, N. Shakhova, L. Matveev, V. Zaitsev, A. Matveyev, E. Zagaynova, V. Gelikonov, N. Gladkova, A. Vitkin, and G. Gelikonov, "Optical coherence tomography-based angiography device with real-time angiography B-scans visualization and hand-held probe for everyday clinical use," *J. Biophotonics* 11(10), e201700292 (2018).
62. M. Y. Kirillin, P. D. Agrba, and V. A. Kamensky, "In vivo study of the effect of mechanical compression on formation of OCT images of human skin," J. Biophotonics **3**(12), 752–758 (2010).
63. N. Matsumoto, N. Saito, K. Miyoshi, M. Nakanishi, and M. Fukuda, "Combination effect of hyperthermia and photodynamic therapy on carcinoma," Arch. Otolaryngol., Head Neck Surg. **116**(7), 824–829 (1990).
64. H. Kurokawa, H. Ito, M. Terasaki, and H. Matsui, "Hyperthermia enhances photodynamic therapy by regulation of HCP1 and ABCG2 expressions via high level ROS generation," Sci. Rep. **9**(1), 1638 (2019).
65. B. W. Henderson, S. M. Waldow, W. R. Potter, and T. J. Dougherty, "Interaction of photodynamic therapy and hyperthermia: tumor response and cell survival studies after treatment of mice in vivo," Cancer Res. **45**, 6071 (1985).
66. Y. H. Ong, M. M. Kim, and T. C. Zhu, "Photodynamic therapy explicit dosimetry," Chapter 3 in *Recent Advancements and Applications in Dosimetry*, Ed. M. F. Chan, Nova Science Publishers, 2018.
67. J. C. Finlay, S. Mitra, M. S. Patterson, and T. H. Foster, "Photobleaching kinetics of Photofrin in vivo and in multicell tumour spheroids indicate two simultaneous bleaching mechanisms," Phys. Med. Biol. **49**(21), 4837–4860 (2004).
68. M. Weston and M. Patterson, "Monitoring oxygen concentration during photodynamic therapy using prompt photosensitizer fluorescence," Phys. Med. Biol. **58**(20), 7039–7059 (2013).
69. K. Szaciłowski, W. Macyk, A. Drzewiecka-Matuszek, M. Brindell, and G. Stochel, "Bioinorganic photochemistry: frontiers and mechanisms," Chem. Rev. **105**(6), 2647–2694 (2005).
70. I. Yoon, J. Z. Li, and Y. K. Shim, "Advance in photosensitizers and light delivery for photodynamic therapy," Clin. Endosc. **46**(1), 7–23 (2013).